Eur. Phys. J. B **3**, 421–426 (1998)

THE EUROPEAN PHYSICAL JOURNAL B

© EDP Sciences
Springer-Verlag 1998

Charge density wave transport in submicron antidot arrays in $NbSe_3$

Yu.I. Latyshev[1,2], B. Pannetier[1], and P. Monceau[1,a]

[1] Centre de Recherches sur les Très Basses Températures, Laboratoire associé à l'Université Joseph Fourier, CNRS, BP 166, 38042 Grenoble Cedex 9, France
[2] Institut of Radioengineering and Electronics, Russian Academy of Sciences, Mokhovaya 11, 103907 Moscow, Russia

Received: 25 November 1997 / Received in final form: 30 March 1998 / Accepted: 6 April 1998

Abstract. We demonstrate for the first time that a periodic array of submicrometer holes (antidots) can be patterned into thin single $NbSe_3$ crystals. We report on the study of Charge Density Wave (CDW) transport of the network of mesoscopic units between antidots. Size of the elementary unit can be as small as 0.5 μm along the chain axis and 0.2 μm $\times$ 0.3 μm in cross-section. We observe size effects for Ohmic residual resistance and in CDW transport current-voltage characteristics in submicronic networks.

PACS. 71.45.Lr Charge-density-waves systems – 73.20.Mf Collective excitations (including plasmons and other charge-density excitations) – 73.23.Ps Other electronic properties of mesoscopic systems

1 Introduction

There is a considerable interest in the study of mesoscopic CDW structures the characteristic size of which is comparable with the coherence length for the phase or the amplitude of the CDW order parameter. From these studies it is expected to obtain new informations about the intrinsic coherence of the CDW conduction [1]. Recent experimental and theoretical investigations have demonstrated the possibility of the observation of quantum interference effects in heterostructures [2,3] and nanostructures [4] in CDW materials. Progress in mesoscopic CDW studies is foreseeable with the recent development of epitaxial thin film technology [5] combined with electron lithography technique. In the present publication, we report on CDW transport in submicron structures patterned on thin single crystal of the CDW quasi one-dimensional (Q1D) compound $NbSe_3$.

2 Experimental

The idea of the experiment was to carry out the realization of a mesoscopic structure in which CDW motion is localized in an array of small cells with a submicron size, each cell being electrically connected to the neighbouring ones by transverse (to the chains) conduction. We show in Figure 1 a schematic example of such a structure. The chain direction b axis of $NbSe_3$ is along the horizontal axis and the c axis along the vertical one. A triangular lattice of holes (antidots) is made in such a way that the projection of holes along the y direction overlaps, that provides small units of CDW conduction between neighbouring holes. The individual cell is shown in Figure 1 as a shaded rectangle.

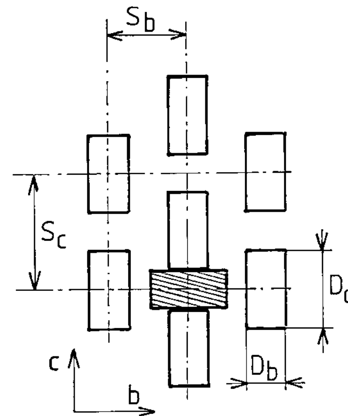

Fig. 1. Schematic picture of the structure with a triangle lattice of holes (antidots). The chain axis is along the X-direction. The projections of holes along the Y-direction overlap in order to block CDW motion in a cell between neighboring holes. Elementary CDW conducting unit is shown as the shaded rectangle.

We selected the most perfect thin $NbSe_3$ crystals with a thickness, d, less than 1 μm and a relatively large width w ($w > 20$ μm). The width is along the c crystallographic axis. The $NbSe_3$ crystals were first glued onto a silicon or sapphire substrate using a fluid resist. After baking

[a] e-mail: `monceau@labs.polycnrs-gre.fr`

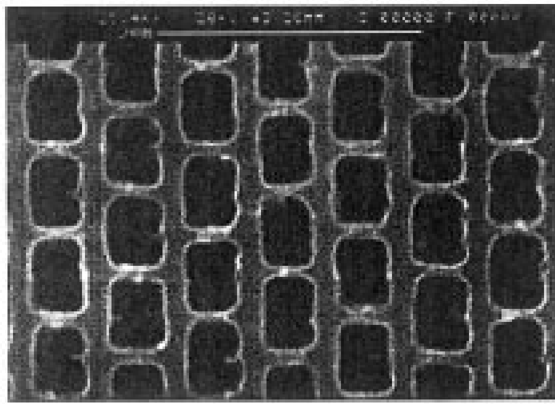

b

(a)

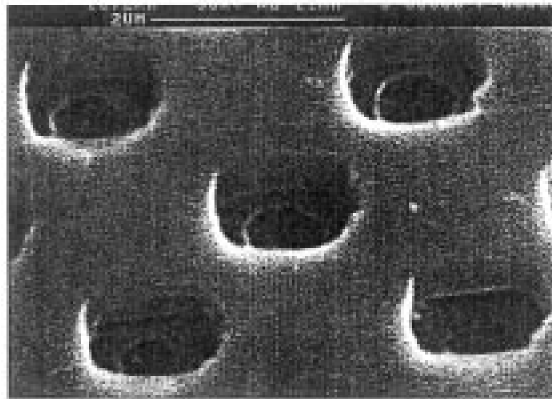

b

(b)

Fig. 2. Scanning electron micrographs of the patterned part of $NbSe_3$. The direction of chains (b axis) is along horizontal axis. (a) sample # 1 on a sapphire substrate (top view), (b) sample # 2 on a silicon substrate (oblique view).

10 minutes at 130 °C the residues of resist were removed by a soft oxygen plasma etching.

The desired holes have high aspect ratio since they must pierce the whole thickness of the crystal. One therefore uses anisotropic reactive ion etching (low pressure SF_6) through an aluminum metallic mask. For its fabrication we have preferred to avoid the standard lift-off technique which could damage the fragile crystal. Rather we have used the following non conventional technique: we first spin on a PMMA layer of nominal thickness 0.5 μm and bake it at 160 °C during 10 minutes. This resist layer is then patterned by direct writing with the electron beam of a scanning electron microscope and developed. A 50 nm aluminum mask is then prepared on top of the patterned PMMA layer by angle evaporation. With proper choice of the angle (typically $\pm 45°$) the small holes patterned in the resist were accurately transfer to the Al mask. The etching of $NbSe_3$ is then achieved in a SF_6 plasma through the aluminum film. We have checked optically that for most of the samples the depth of etching coincides with the thickness of the crystal itself. We finally remove the aluminum mask by wet etching and the PMMA layer in an oxygen plasma.

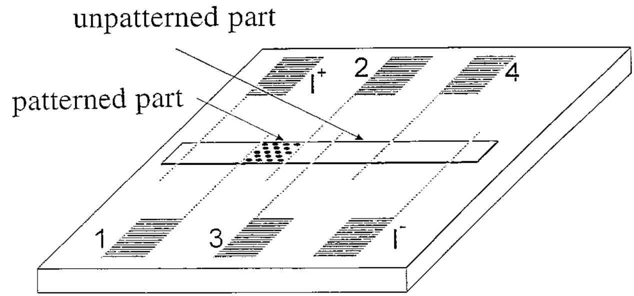

Fig. 3. The geometry of the experiment.

Most of the experimental results presented in this paper were obtained on sample # 1 whose micrograph is shown in Figure 2a. Sample # 1 was glued on a sapphire substrate and was first thinned using SF_6 reactive ion etching down to about 0.5 μm. For this particular sample a 25 nm thin silicon layer was first deposited by e-beam evaporation in order to evacuate charges in the subsequent e-beam lithography. The layer was removed at the end of the process. The patterned holes (hereafter called antidots) have a rectangular shape and are repeated according to a triangular lattice as designed in Figure 1. The periodicity of the lattice of antidots is $S_b = S_c = 0.6$ μm with a rectangular hole cross-section with $D_b = 0.3$ μm along the b axis and $D_c = 0.4$ μm along the c axis (see Fig. 2a).

Four gold contact pads are then patterned in a second e-beam lithographic step using lift-off technique. External leads are attached to the gold strips using indium contacts. The contact geometry is chosen to allow measurements on adjacent patterned and non-patterned zones (typical length: 100 μm) of the same crystal as drawn in Figure 3. The microhole structure covers the whole width of the crystal.

A few additional measurements were performed on a second crystal having larger hole sizes: sample # 2 (Fig. 2b). This sample, 0.4 μm thick, was glued onto a silicon substrate. Here the pattern consists of a square lattice of (nominally) circular holes. The actual hole diameter is about 1.5 μm and the lattice periodicity is 3.4 μm.

The electrical resistance and the differential current voltage characteristics were measured with a 40 Hz phase sensitive bridge using the inner probes 1-2 and 3-4 as voltage probes to compare the properties of the patterned and non-patterned segments.

All the sample parameters are indicated in Table 1.

Table 1. Dimensions of the individual hole and of the periodicity of the antidot array (see Fig. 1) for sample # 1 and # 2. Dimensions of the samples are also indicated.

Sample	Hole parameters μm		Spacing μm		Patterned zone μm		Unpatterned zone μm	
	D_b	D_c	S_b	S_c	Length	Width	Length	Width
#1	0.3	0.4	0.6	0.6	70	22	620	22
#2	1.5	1.4	3.0	3.7	80	130	540	130

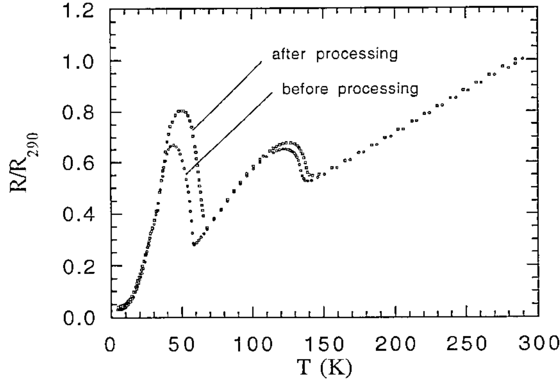

(a)

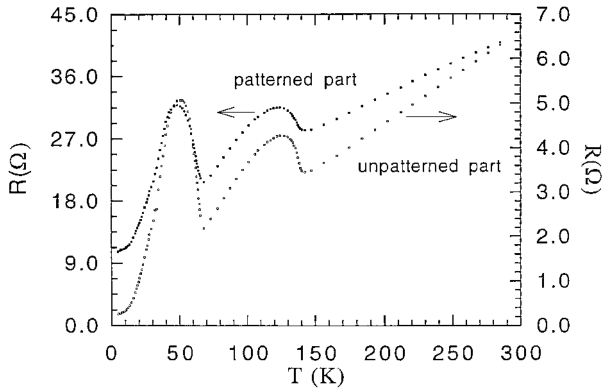

(b)

Fig. 4. Temperature dependences of the resistance of $NbSe_3$ (sample # 1), (a) before and after processing (baking the PMMA layer at 160 °C), (b) of the patterned and unpatterned part after processing.

3 Results

In what follows, each $NbSe_3$ sample measured is processed (essentially baking of the PMMA layer at 160 °C) on its total surface, but only a part is patterned (antidot array) as shown in Figure 3.

The processing treatment yields some changes in the properties of the $NbSe_3$ samples. In Figure 4a we show the temperature dependence of a $NbSe_3$ sample before processing and after processing. The consequences of processing are an increase of both Peierls transition temperatures ($T_{P_1} = 145$ K and $T_{P_2} = 59$ K for pure $NbSe_3$ crystals), an increase of the resistance at both maxima in the $R(T)$ dependence and a larger residual resistance at low temperatures. However the sample still conserves all the properties of a relatively good quality $NbSe_3$ crystal. After processing but without patterning the resistance ratio $R(290\text{ K})/R(4.2\text{ K})$ is in range of ~25-40 and the threshold electric field for CDW depinning at 50 K is $E_T \sim 100$ mV/cm.

Patterning the antidot array strongly affects the resistance of the $NbSe_3$ sample. The sheet resistance of the patterned part increases considerably, for instance by a factor 6.5 at room temperature for sample # 1; however the Peierls transition temperatures are not changed with respect to the unpatterned part as shown in Figure 4b. The effect of patterning is clearly seen in the temperature dependence of the ratio between the resistance of the patterned part and the resistance of the unpatterned part. Prominent features appear near both Peierls transition temperatures and at low temperatures below 50 K. The decrease of the resistance of the patterned part below 50 K is largely suppressed for sample # 1 with the shorter antidot lattice periodicity. Thus, the resistance ratio between room temperature and helium temperature is 4.8 for sample # 1 and 10 for sample # 2 (to be compared to 25-40 for the unpatterned zone).

Figure 5 shows the variation of the differential resistance $\frac{dV}{dI}$ as a function of the applied current for both non-patterned (Fig. 5a) and patterned (Fig. 5b) parts of sample # 1. CDW motion occurs above a threshold electric field E_T defined as $E_T = \frac{V_T}{L} = \frac{RI_T}{L}$ with R the Ohmic resistance, L the distance between electrodes and I_T the critical current at which non linearity in the $(I-V)$ characteristics appears. It can be noted that I_T for the lower CDW is nearly identical for the patterned and unpatterned parts as shown in Figure 6.

4 Analysis and discussion

We will now describe a simple model in order to explain the properties of submicronic structures patterned on a single $NbSe_3$ crystal. We consider that: 1) transport along chains occurs only in the short cells located between neighbouring holes (shaded part in Fig. 1) and 2) transport

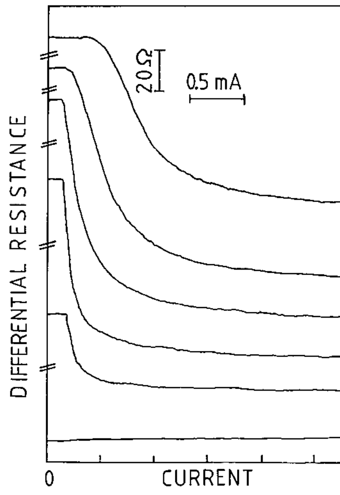

(a)

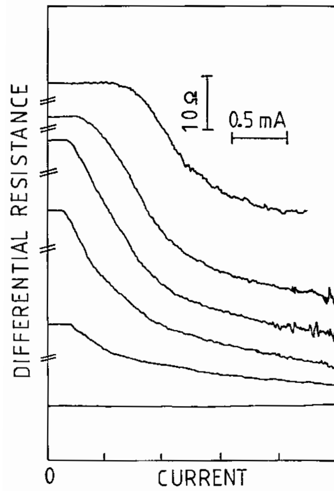

(b)

Fig. 5. Variation of the differential resistance dV/dI, as a function of current, I, for the patterned and the non-patterned parts of $NbSe_3$ (sample # 1). The temperatures from top to bottom are as follows: 38.3, 42.1, 49.8, 56.9, 62.7 and 67.7 K. The corresponding linear resistances (in Ω) are as follows: 105, 106, 118, 107, 87, 76 (for the patterned part) and 118, 141, 151, 139, 98, 66 (for the non-patterned part).

from one cell to the adjacent one requires charge motion perpendicularly to the chains. One can imagine an equivalent scheme which consists in an electrical network with two types of resistances: one, R, for transport along the chains, the other, r, for transport across the chains as drawn in inset of Figure 7.

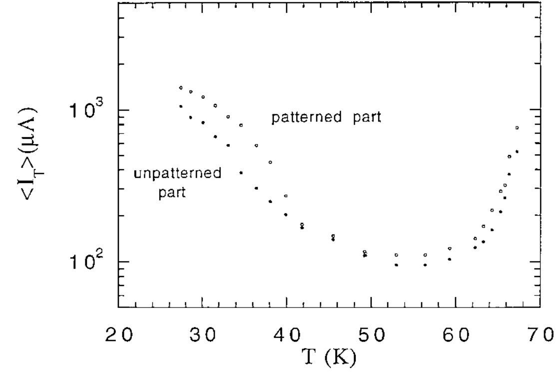

Fig. 6. Temperature dependences of the average threshold current $\langle I_T \rangle$ for initiating the CDW conduction in $NbSe_3$ (sample # 2).

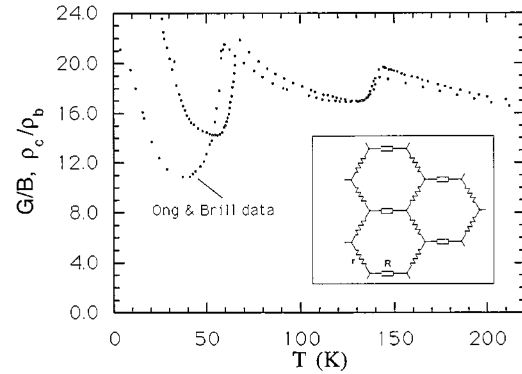

Fig. 7. Temperature dependences of the normalized sheet resistance ratio of the patterned to the non-patterned parts, G/B, for sample # 1 (full squares) and the anisotropy ratio ρ_c/ρ_b measured by Montgomery technique (empty squares) from [6]. The factor $B = 0.43$ normalizes both quantities at the same value at room temperature. Inset: the equivalent electrical scheme of the patterned part.

4.1 Ohmic behaviour

The ratio between the sheet resistance of the patterned part, R, and that of the unpatterned one, R°, $G = \frac{R}{R^\circ}$ can be expressed as a linear function of r/R, which is proportional to the resistivity anisotropy ρ_c/ρ_b (ρ_c: resistivity along the width of the sample, ρ_b: resistivity along the chain axis). Thus, $G = A + B(\rho_c/\rho_b)$ where A and B are coefficients depending on the geometry of the network. In the case where $A \sim 1$ and $\rho_c/\rho_b \gg 1$ which is appropriate in the present case, one can write:

$$G = B\frac{\rho_c}{\rho_b} \cdot \qquad (1)$$

For sample # 1, we find $G = 6.5$ at room temperature. Using the value of $\rho_c/\rho_b \sim 15$ measured at room temperature in $NbSe_3$ [6], one obtains $B = 0.43$. The justification for the validity of our conduction model is shown in Figure 7 where we have drawn the temperature dependence of $\frac{G(T)}{B}$

with $B = 0.43$ and that of the resistivity anisotropy ρ_c/ρ_b measured in [6] using the Montgomery technique. A good agreement between the temperature dependence of both quantities is found in the full temperature range above $T \simeq 55$ K (remember that T_{p1} and T_{p2} are larger in our processed samples). At lower temperatures, equation (1) is unvalid, because the additional contribution to the resistance due to the patterned structure. We consider that the origin of this additional contribution comes from the additional scattering in the mesoscopic units, when the mean free path, ℓ, becomes comparable at low temperatures to the length of the unit along the chains. Using the data from [7] for the carrier mobility along chains, we estimate that ℓ is ~ 0.3 μm at $T = 40$ K. Below this temperature, the increase of ℓ becomes limited by the antidot periodicity. That can explain the decrease of the residual resistance to 4.8 (sample # 1) compared to 10 (sample # 2) when the antidot lattice periodicity along the b axis is 0.6 μm (sample # 1) to be compared to 3 μm (sample # 2).

4.2 Threshold field for CDW depinning

We consider now the CDW depinning in a network structure. The threshold we have defined in Section 3 corresponds to a value averaged over the whole structure. Let it to be noted as: $\langle E_T \rangle = \frac{R}{L}\langle I_T \rangle$.

However, it is also possible to define a local threshold field, noted as E_t, in an elementary cell: the shaded rectangle for the patterned part as shown in Figure 1 with dimensions Λ along the b axis and Λ' along the c axis. If the elementary cell extends half the distance between units along b axis as represented in Figure 1, then $\Lambda = S_b$ and $\Lambda' = S_c - D_c$. For the unpatterned part, the elementary cell is larger with dimensions S_b along the b axis and S_c along the c axis. E_t is connected with the local current I_t, along the chains in that elementary cell such as $I_t = \sigma_b E_t S$ where σ_b is the linear conductivity along the chains and S the cross-section of the sample. The ratio between E_t in the patterned part and the threshold field of the non-patterned part, that one notes as E_t^0, can be expressed as follows:

$$\frac{E_t}{E_t^0} = \frac{I_t}{I_t^0}\frac{\sigma_b^0}{\sigma_b}\frac{S_c}{S_c - D_c}.$$

One then makes the reasonable assumption that the local $\frac{E_t}{E_t^0}$ is the same than the average value for the whole sample $\left\langle \frac{E_T}{E_T^0} \right\rangle$.

For sample # 1 we have shown the temperature dependence of $\langle I_T \rangle$ and $\langle I_T^0 \rangle$ in Figure 6. The temperature variation of $\alpha = \frac{\langle I_T \rangle}{\langle I_T^0 \rangle}$ for sample # 1 and # 2 are drawn in Figure 8.

For sample # 1, with $D_b = 0.3$ μm and $D_c = 0.4$ μm, we measure $\langle I_T/I_T^0 \rangle$=1.2 (Fig. 8). With $\frac{S_c}{S_c - D_c} = 3$, one gets $E_t/E_t^0 \approx 4$, demonstrating that there is a well pronounced size effect for the local E_t in a cell with submicron size. Similar size effects have been previously observed in

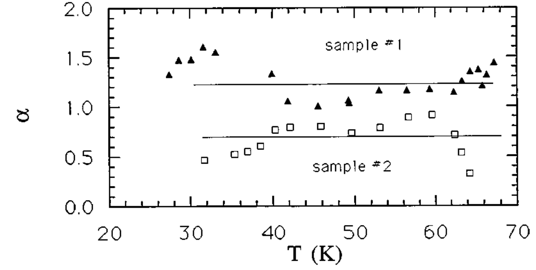

Fig. 8. Temperature dependence of the ratio, α, between average threshold current $\langle I_T \rangle$ and $\langle I_T^0 \rangle$ for the patterned and unpatterned parts of $NbSe_3$ (sample # 1 and # 2).

TaS_3 single crystals with a very small cross-section [8] and a short length [9].

For sample # 2, with a larger cell size ($D_c = 1.4$ μm, $D_b = 1.5$ μm), we find that $\langle I_t/I_T^0 \rangle \sim 0.7$. For this sample, $\frac{S_c}{S_c - D_c} = 1.6$; one neglects any size effect for σ_b such as $\sigma_b^0/\sigma_b \sim 1$. Then $E_t/E_t^0 \sim 1.1$ not far from the value of 1.

4.3 Current conversion

One of the aims of our study is the conduction due to CDW motion in a submicron unit. The process of conversion of the normal carrier current into a CDW current is still not well understood. In several theoretical models the conversion process is accompanied by auto-localization of carriers [10], formation of phase-slippage centers [11], dynamical amplitude solitons [12], tunneling between solitons under the barrier [13].

Phase slippage at current injection electrodes has resulted from experiments in which the variation of the threshold voltage was studied as a function of the distance between electrodes. It was found [14], that:

$$V_T = E_p L + V_0.$$

The first term corresponds to the bulk pinning due to impurities and the extra term V_0 was interpreted as the potential necessary for the nucleation of a CDW dislocation loop for conversion of normal current into the CDW condensate. Typically for $NbSe_3$ V_0 is in the range of 0.2-0.5 mV at T = 40 K [14].

One can estimate the threshold voltage in our elementary cell of the patterned zone. The local critical current is the total critical current $\langle I_T \rangle$ divided by the number of channels along c axis. The resistance of the elementary cell can be calculated according to its dimensions and the conductivity at the given temperature. Thus, one estimate that at 40$\sim$50 K, the threshold voltage in the elementary cell is in the range of 50$\sim$100 μV, much less than V_0. One are led to conclude that in our network geometry with submicronic dimensions where the current is fed to the elementary cell without any interface with a normal metal, there is no vortex dislocation loop generated.

The other models [10,12,13] estimate the conversion length, L_{conv}, to be of the order of $\hbar v_F/\Delta$ (Δ: the CDW

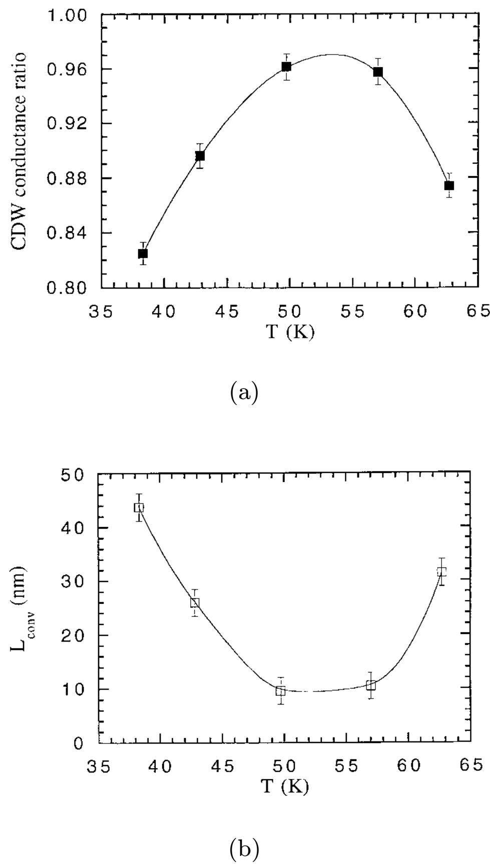

Fig. 9. (a) Temperature dependence of the ratio of the CDW conduction in the submicron unit (shaded rectangle in Fig. 1) and in the equivalent bulk part for applied current 10 times the average threshold value for $NbSe_3$ (sample # 1). (b) Temperature dependence of the conversion length L_{conv} for normal carriers into CDW current (sample # 1). For the procedure to extract L_{conv} from data, see text. Full lines are guides for eyes.

gap). An estimate of L_{conv} for $NbSe_3$ is $\sim$ 20 nm. One can expect to determine a value of the conversion length from experiments on short samples with a length Λ comparable with L_{conv}. In such a short sample only a part of the length of the sample, Λ-2L_{conv}, contributes to the non-linear conduction. A comparison with a macroscopic sample with the same thickness and the same ratio length/width can be made. It is then expected that in small samples the maximum contribution to the non-linear conduction will be at least $\frac{\Lambda-2L_{conv}}{\Lambda}$ smaller.

We have measured the non-linear properties in the current regime where the CDW conduction saturates *i.e.* $I \approx 10\langle I_T\rangle$ for both patterned and unpatterned parts of sample # 1. We obtain that the CDW conductivity in an individual cell, σ_{CDW}, is always smaller in the patterned part of the sample with respect to the value in the non-patterned part of the same sample, σ^0_{CDW}. Figure 9a shows the temperature dependence of $\gamma = \sigma_{CDW}/\sigma^0_{CDW}$. Making the suggestion that this ratio γ is a measurement of $\frac{\Lambda-2L_{conv}}{\Lambda}$, one can estimate L_{conv} as equal to $\frac{\Lambda(1-\gamma)}{2}$. That yields a value of L_{conv} of $\sim$ 10-20 nm the temperature variation of which is drawn in Figure 9b. This estimate of L_{conv} is in reasonable agreement with the theoretical calculations [10,12,13].

5 Conclusions

We have realized submicron antidot arrays in thin single $NbSe_3$ crystals. The comparison between the transport properties respectively in the patterned and unpatterned parts of the crystal reveals specific features of Ohmic conduction and CDW transport in submicron units.

The work was partly supported by the Russian State Program "Physics of Solid State Nanostructures" (project Nr 97.1052) and by CNRS through the PICS Nr. 153.

References

1. For reviews in charge density wave properties in quasi-one-dimensional conductors: *Electronic Properties of Inorganic Quasi-One-Dimensional Compounds* Parts 1 and 2, edited by P. Monceau (D. Reidel, Boston, 1985); G. Grüner, Rev. Mod. Phys. **60**, 1129 (1988).
2. A.A. Sinchenko, Yu.I. Latyshev, I.G. Gorlova, P. Monceau, Pis'ma Zh. Eksp. Teor. Fiz. **64**, 259 (1996); JETP Lett. **64**, 285 (1996).
3. B. Rejaei, G.E.W. Bauer, Phys. Rev. B **54**, 8487 (1996).
4. Yu.I. Latyshev, O. Laborde, P. Monceau, S. Klaumuenzer, Phys. Rev. Lett. **78**, 919 (1997).
5. H.S.J. van der Zant, O.C. Mantel, C. Dekker, J.E. Mooij, C. Traeholt, Appl. Phys. Lett. **68**, 3823 (1996).
6. N.P. Ong, J.W. Brill, Phys. Rev. B **18**, 5265 (1978).
7. N.P. Ong, Phys. Rev. B **18**, 5272 (1978).
8. D.V. Borodin, S.V. Zaitsev-Zotov, F.Ya. Nad', Zh. Esp. Teor. Fiz. **93**, 1394 (1987); Sov. Phys. JETP **66**, 793 (1987).
9. S.V. Zaitsev-Zotov, V.Ya. Pokrovskii, J.C. Gill, J. Phys. I France **2**, 111 (1992).
10. S.A. Brazovskii, Zh. Eksp. Teor. Fiz. **78**, 677 (1980); Sov. Phys. JETP **51**, 342 (1980).
11. L.P. Gor'kov, Zh. Eksp. Teor. Fiz. **86**, 1818 (1984); Sov. Phys. JETP **59**, 1057 (1984).
12. S.N. Artemenko, A.F. Volkov, A.N. Kruglov, Zh. Eksp. Teor. Fiz. **91**, 1537 (1986); Sov. Phys. JETP **64**, 906 (1986).
13. I.V. Krive *et al.*, Pis'ma Zh. Eksp. Teor. Fiz. **46**, 99 (1987); JETP Lett. **46**, 121 (1987).
14. P. Monceau, M. Renard, J. Richard, M.C. Saint-Lager, Physica **143B**, 64 (1986).